Supplementary Materials for

Collective modification of photochemical dynamics through strong light-matter coupling

Rana Lomlu,[1] Kelly Leiby,[1] and Andrew J. Musser[1]*

[1]Department of Chemistry and Chemical Biology, Cornell University; Ithaca, NY, 14850, USA.

*Corresponding author. Email: ajm557@cornell.edu

Table of Contents

Supplementary Section 1: Steady-state characterization of bare films
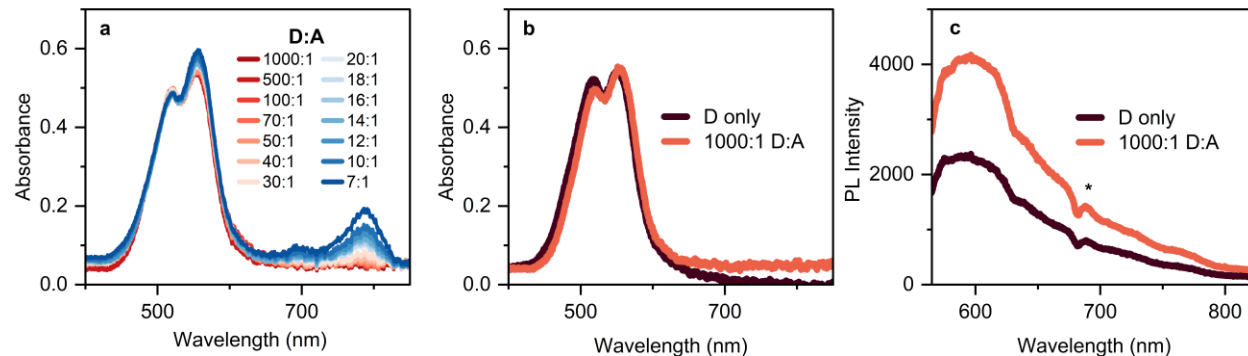

Figure S1: a) Steady state absorption measurements on bare films with varying **D**:**A**. **b)** In the absence of acceptor (**A**), we observe the characteristic signature of aggregated Rhodamine 6G (**D only** trace),[1–3] an enhanced absorption peak at 500 nm. Addition of even a small amount of acceptor noticeably suppresses this effect. **c)** We observe that the emission intensity of 1000:1 **D**:**A** film is higher than the **D**-only film, further suggesting that introducing a small amount of acceptor prevents aggregation. The dips marked by asterisk in the PL spectra (here, as well as in following sections) are due to the dead pixel in the ICCD camera used in the PL experiments.

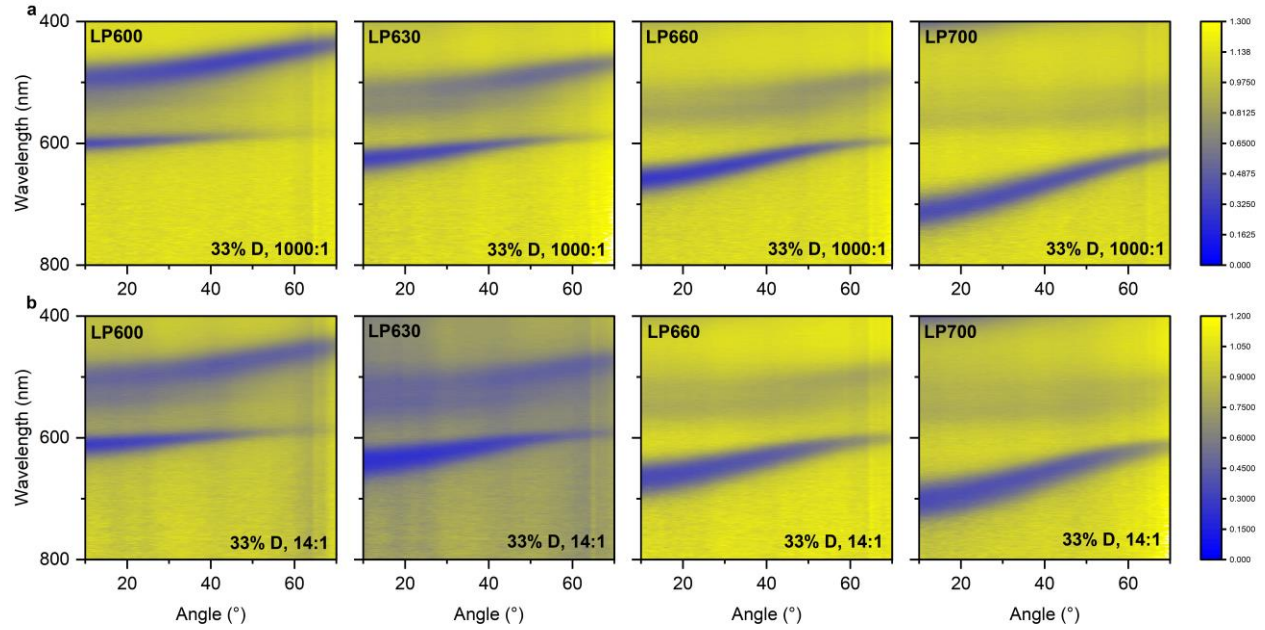**Supplementary Section 2:** Angle-resolved reflectivity measurements of microcavities

Figure S2: Angle-resolved reflectivity maps for microcavities with 33% **D**, showing the detuning range covered for **D:A a)** 1000:1 and **b)** 14:1, respectively. The reflectivity maps demonstrate that the behavior of the lower polariton (LP) remains the same regardless of the acceptor concentration, [**A**], i.e. **A** remains in all cases in the weak-coupling regime.
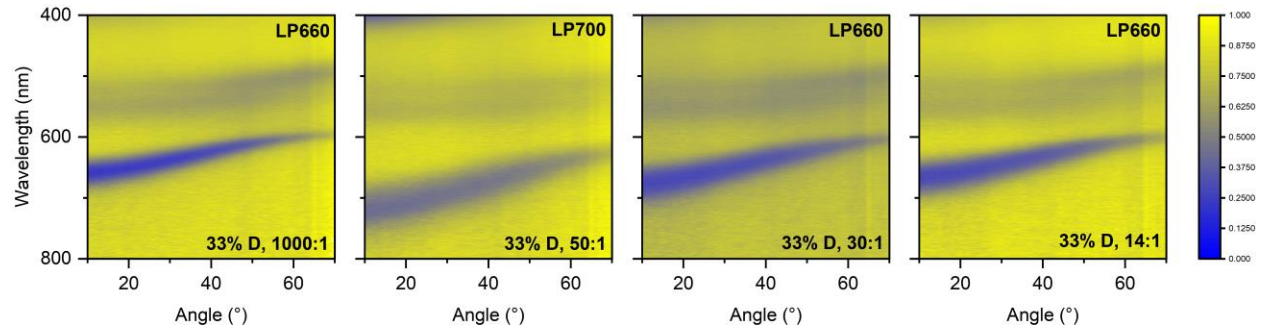

Figure S3: Angle-resolved reflectivity maps for microcavities with 33% **D**, with increasing **A** concentration from left to right (**D:A** 1000:1, 50:1, 30:1, 14:1)

Figure S4: Angle-resolved reflectivity maps for microcavities with 14% **D**, with increasing **A** concentration from left to right (**D:A** 1000:1, 50:1, 30:1, 14:1)
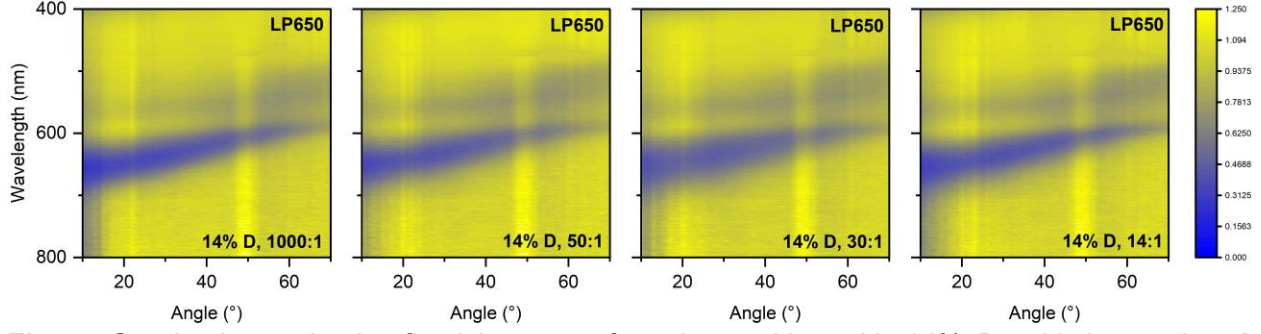

Figure S5: Angle-resolved reflectivity maps for microcavities with 67% **D**, with increasing **A** concentration from left to right (**D:A** 1000:1, 50:1, 30:1, 14:1)
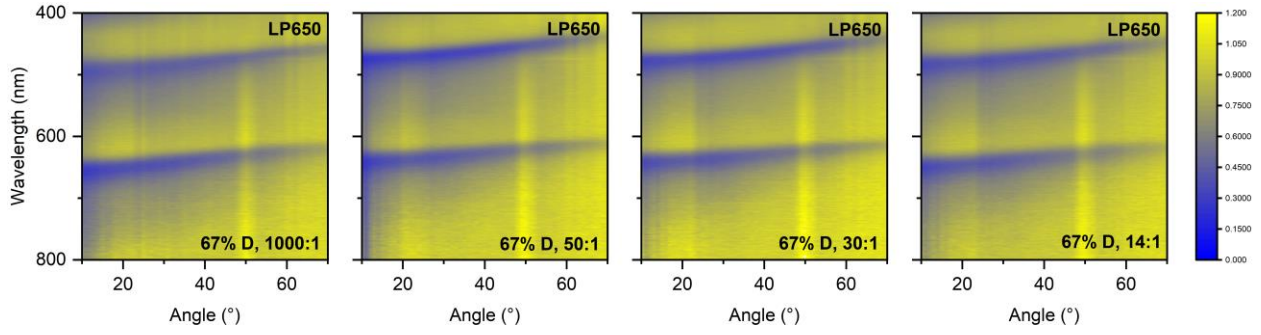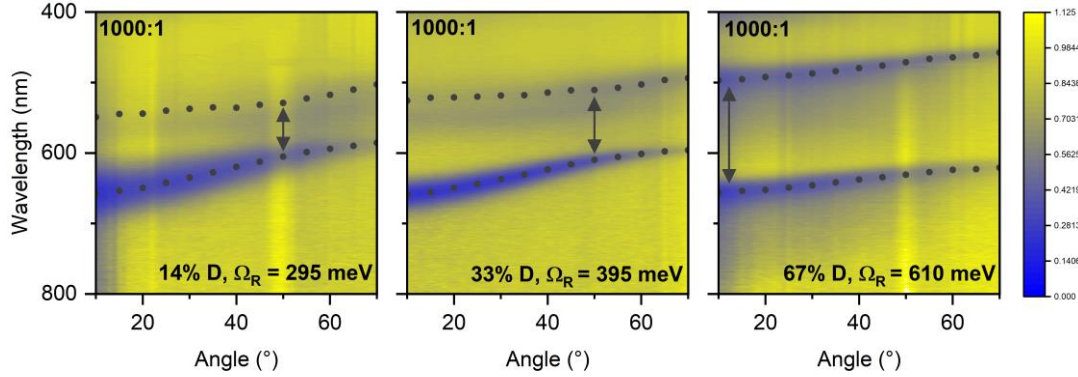

Figure S6: Rabi splitting comparison for microcavities with 14, 33, 67% **D** at LP650. The data points indicate the peak position of the UP and LP at every 5º. Rabi splitting values are extracted from the minimum separation between the UP and LP branches, denoted by arrows.
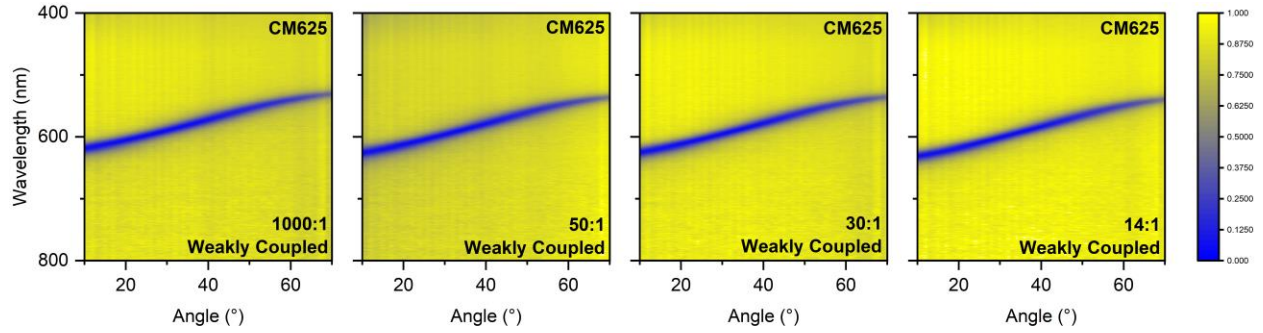
Figure S7: Angle-resolved reflectivity maps for weakly coupled microcavities (from left to right: **D:A** 1000:1, 50:1, 30:1, 14:1). The reflectivity maps do not demonstrate any anticrossing behavior as the mode passes the **D** absorption maximum, highlighting that there is no strong coupling.
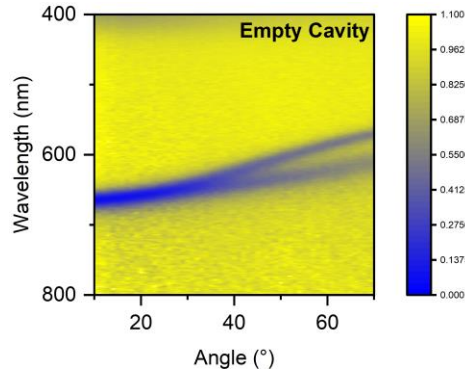

Figure S8: Angle-resolved reflectivity map for a reference empty cavity. The two modes here are observed since this angle-resolved reflectivity measurement was performed with a different polarizer configuration.

Supplementary Section 3: Photoluminescence quenching measurements and Stern-Volmer analysis
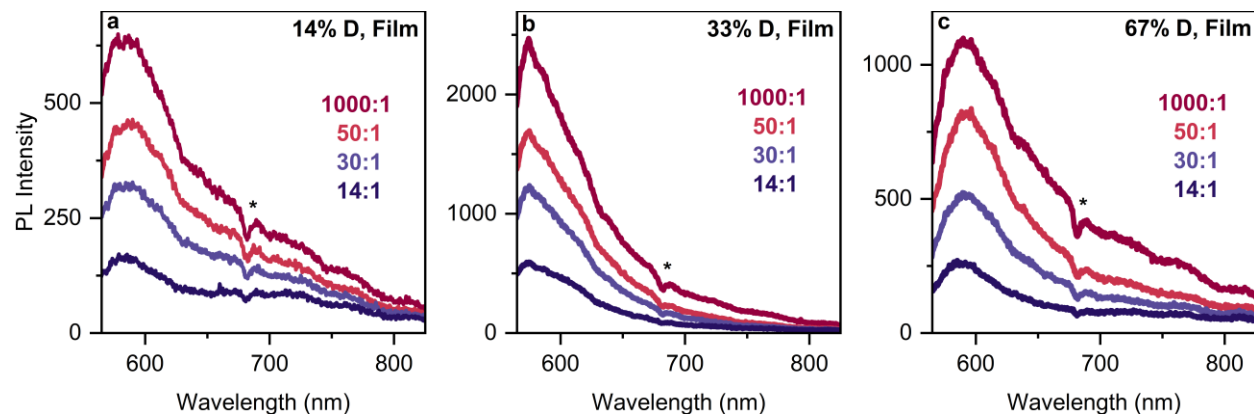
Figure S9: PL emission spectra demonstrating quenching in bare films with **a)** 14% **D**, **b)** 33% **D**, **c)** 67% **D**.

Figure S10: Averaged PL spectra of LP emission in microcavities with **a)** 14% **D**, **b)** 33% **D**, **c)** 67% **D** at 640-650 nm. We measured the emission at 2-6 different spots on each microcavity and averaged the obtained spectra within given wavelength ranges (solid lines). Standard deviation is indicated by shaded areas around the spectra.

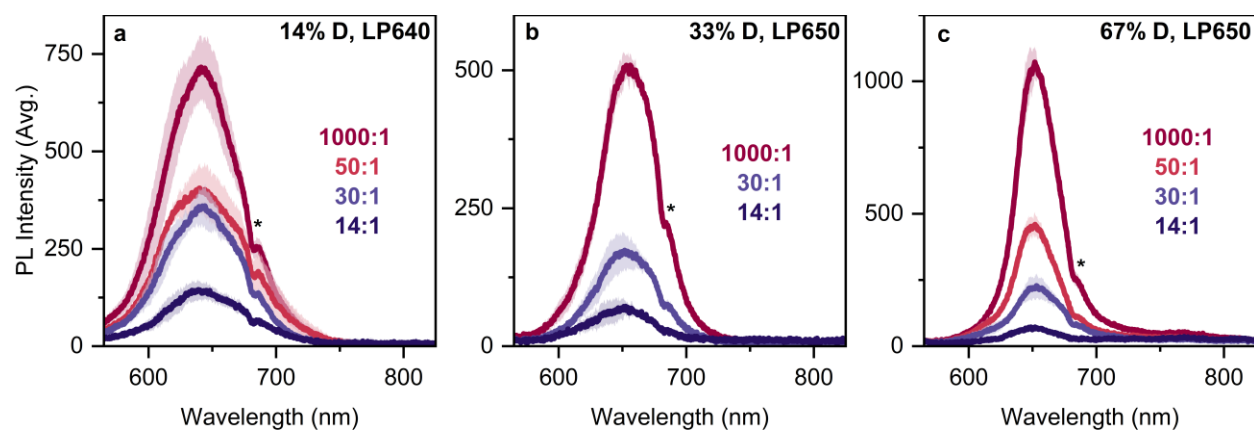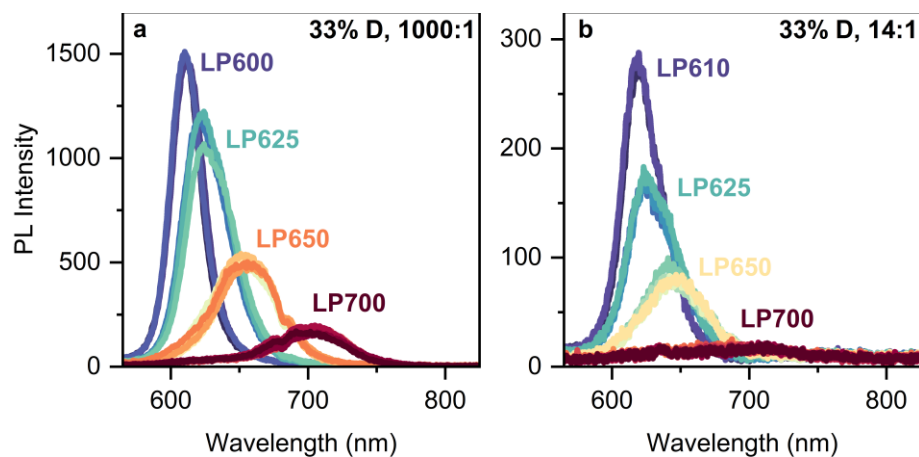**Figure S11:** Detuning dependence of LP emission for 33% **D** microcavities with **D:A a)** 1000:1 and **b)** 14:1. For each **D:A**, the spacer wedge spans 4 microcavities in total, resulting in different detuning values. The given LP emission spectra are measured over 4 microcavities, for both **D:A** 1000:1 and 14:1.
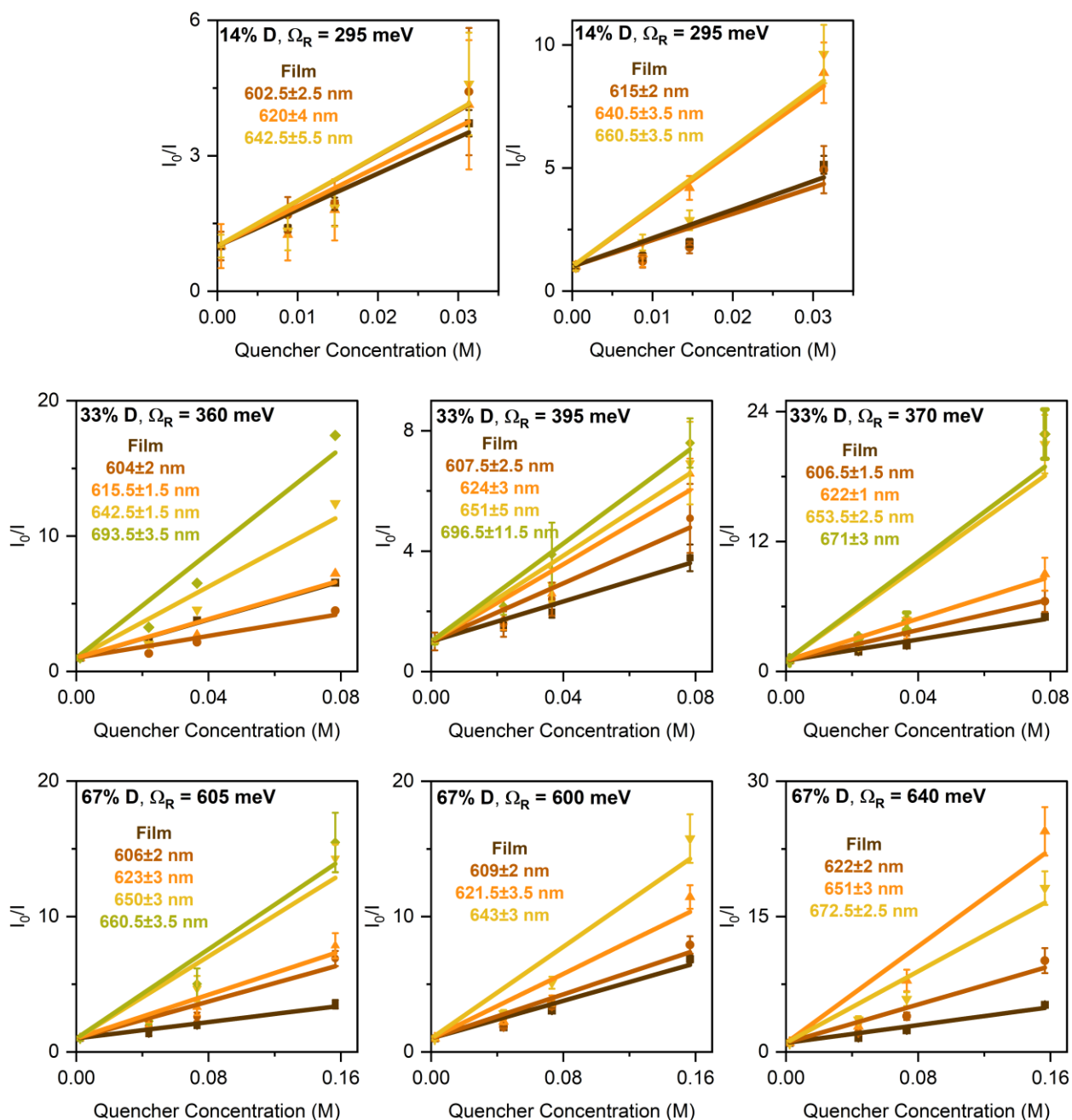
Figure S12: Stern-Volmer analyses of all sample sets of bare films and microcavities with 14, 33, and 67% **D**. The slight variation in Ω_R across reflects batch-to-batch variation in cavity fabrication. All cavities are referenced against their own bare films prepared in the same batch, under identical conditions. All Stern-Volmer plots follow the same **D:A** series of 1000:1, 50:1, 30:1, and 14:1, with the absolute quencher concentration determined by the concentration of donor. Error bars are obtained by averaging 2-10 points measured on the same sample for each data point.

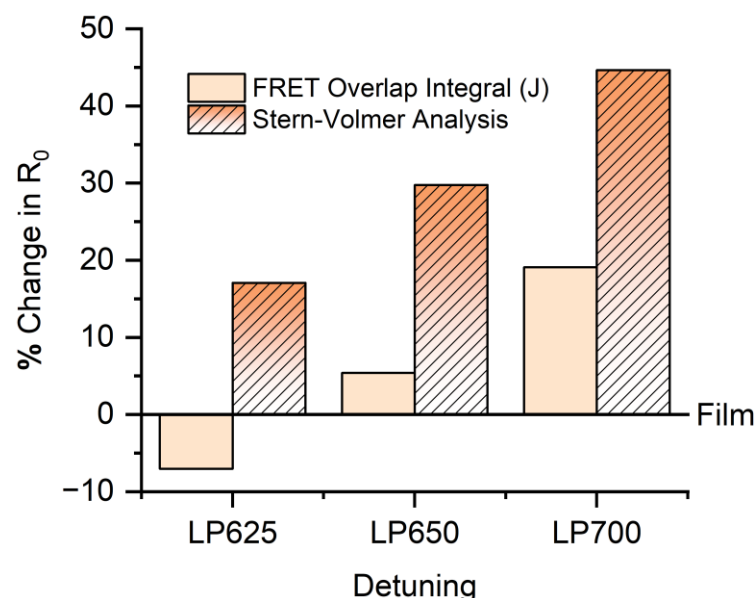**Figure S13:** Percent change in Förster radii (R_0) relative to film-R_0, for various detunings calculated by two different methods. Förster radius is given by the distance between **D** and **A** molecules at which the energy transfer efficiency (or I/I_0) is 50%. Hence, extracting (slope)$^{-1}$ from the Stern-Volmer plots yield the quencher concentration at which the efficiency is 50%. From here, we calculated the approximate distance between **D** and **A** molecules using a simple cubic approximation. We used the experimental results of the 33% **D** for this calculation. To calculate FRET overlap integral J, we used area-normalized emission of **D** and molar absorption coefficient of **A**.[4] We then obtained the relative Förster radii using the relation $R_0 \propto J^{1/6}$, normalizing against the film-R_0 to predict the degree of enhancement. The overlap integral calculation alone is evidently not sufficient to explain the observed enhancement in the Förster radius based on our photoluminescence quenching experiments.

Supplementary Section 4: Time-resolved experiments

All TA measurements were performed with 532nm excitation wavelength resonant with the donor absorption, unless otherwise specified. White rectangles are overlaid on the pump scatter regions in the presented TA heatmaps.
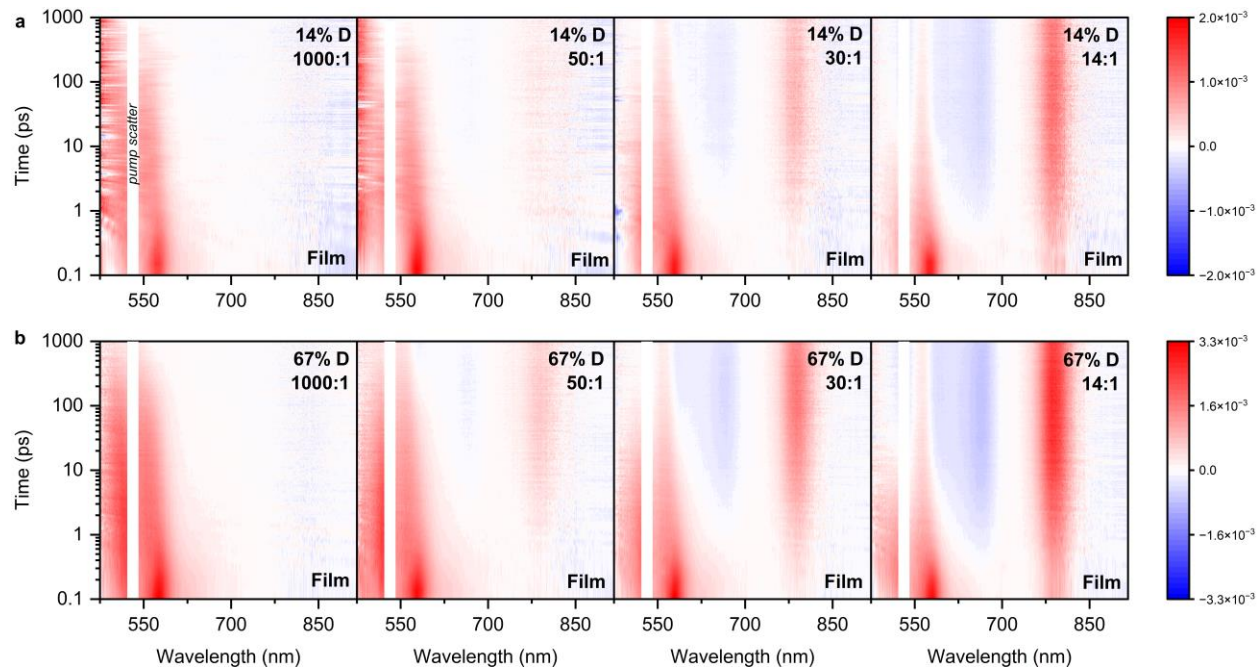

Figure S14: TA measurements on bare films (ΔT/T) with **a)** 14% and **b)** 67% **D**, increasing **A** concentration from left to right.

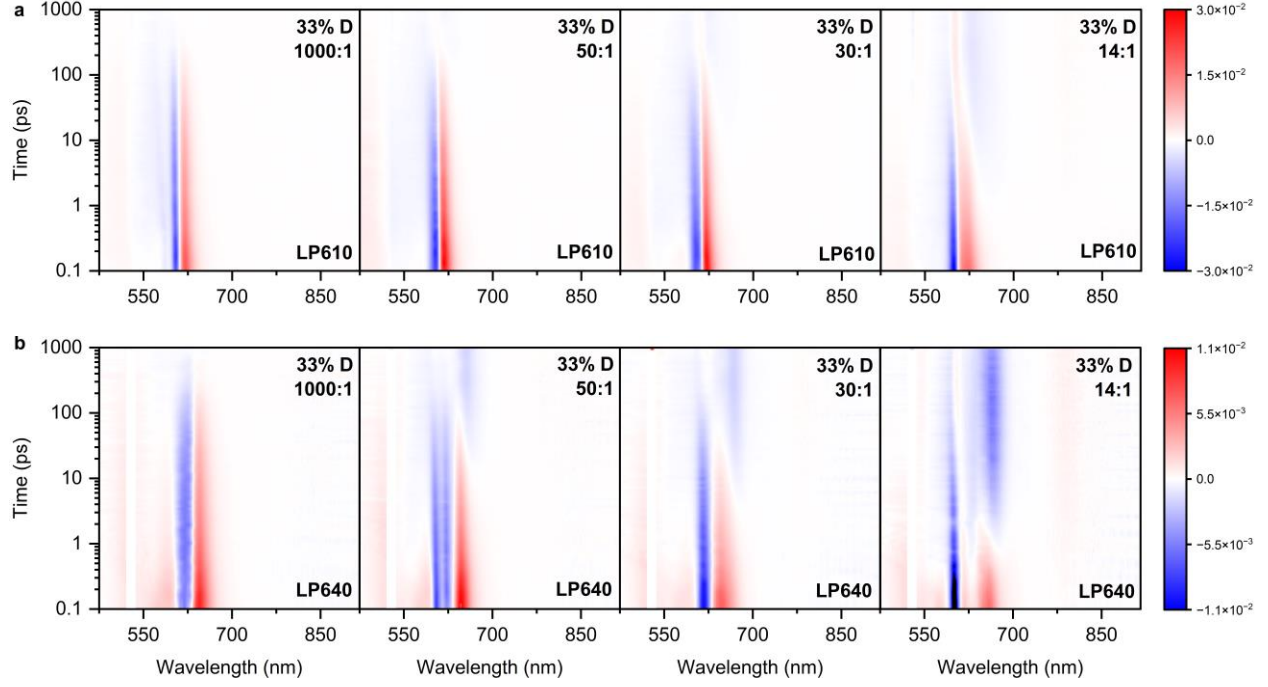**Figure S15:** TA heatmaps of microcavities (ΔR/R) with 33% **D** (as presented in the main text) at **a)** LP610 and **b)** LP640. Population kinetics extracted from the 14:1 heatmaps are presented in main-text Figure 5b.
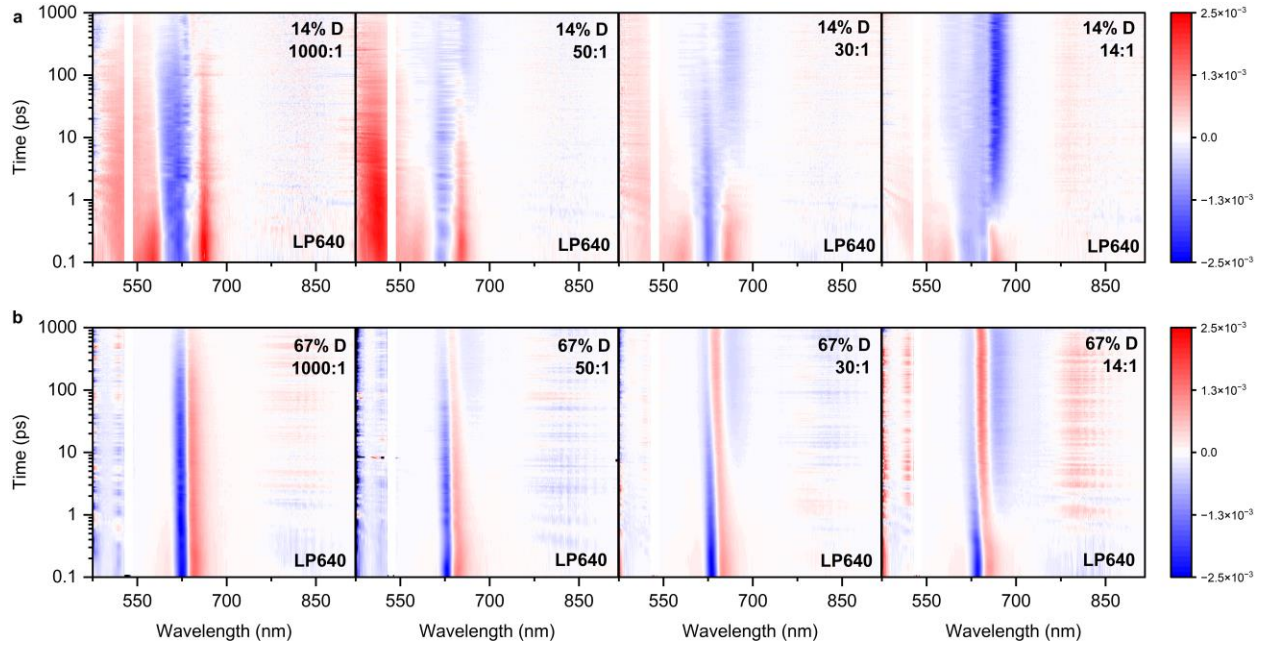

Figure S16: TA heatmaps of microcavities (ΔR/R) with **a)** 14% and **b)** 67% **D**, at LP640. We observe that changing %**D** (and thus Ω_R) doesn't have a substantial impact on dynamics.

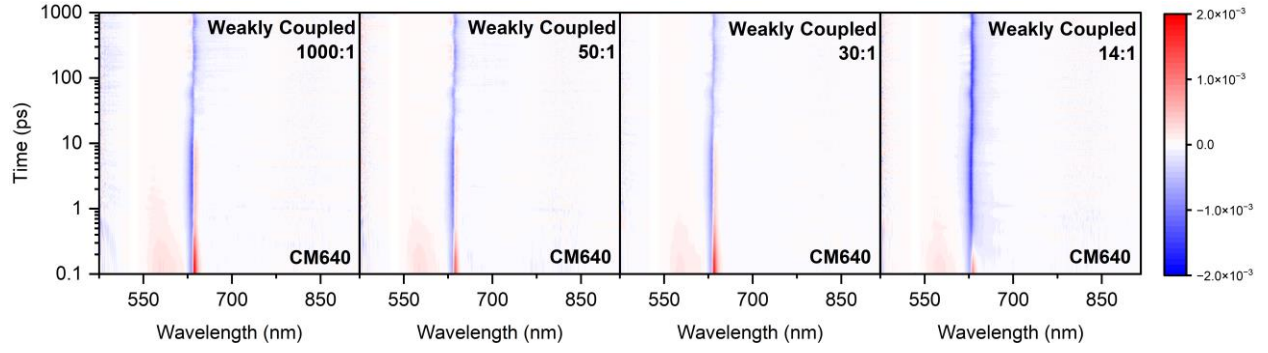**Figure S17:** TA heatmaps of weakly coupled microcavities (ΔR/R) with the photonic mode positioned at 640nm. We do not observe any enhancement effects here as opposed to strongly coupled microcavities.

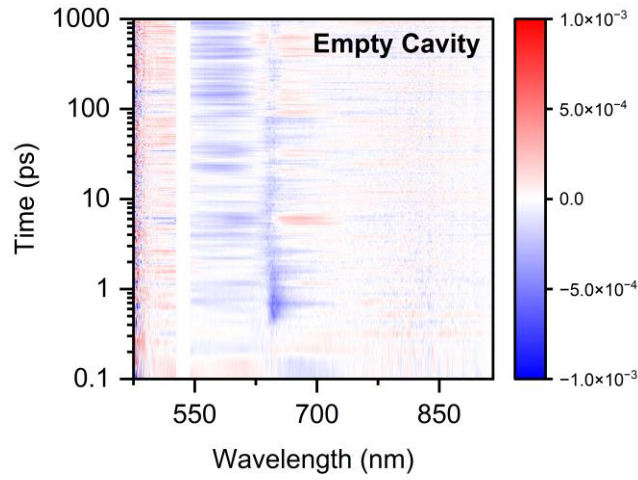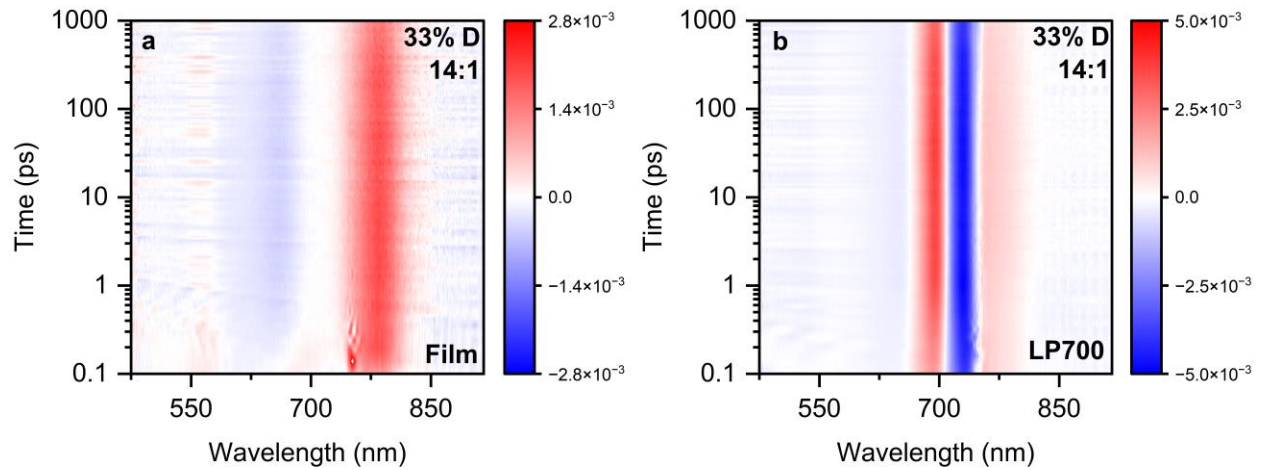**Figure S18:** TA heatmap of an empty cavity (ΔR/R) with cavity mode around 640 nm.

Figure S19: Direct excitation of **A** with 750nm pump for 14:1 **a)** bare film (ΔT/T) and **b)** full **D:A** microcavity (ΔR/R).

Supplementary Section 5: Spectral decomposition and extracted kinetics
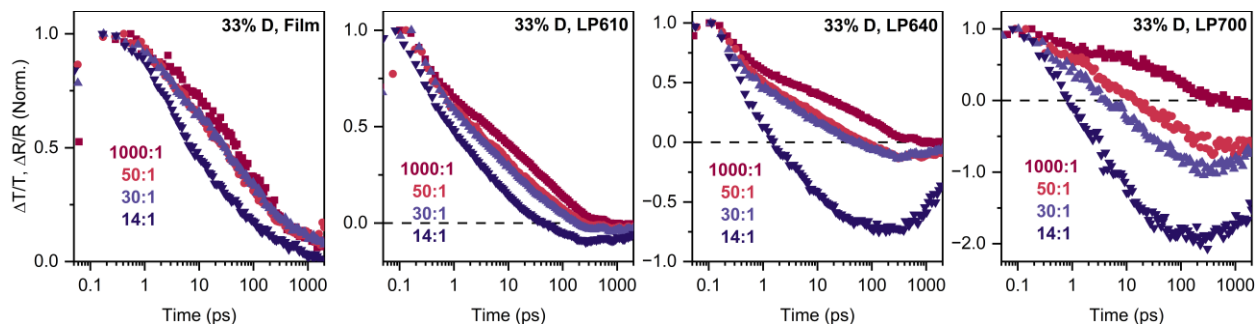
Figure S20: Concentration dependence: extracted kinetics from bare films and microcavities with different detunings (left to right: Film, LP610, LP640, LP700). Film kinetics are extracted from the ground state bleach (GSB) peak of **D**, while all microcavity kinetics are selected at the positive features around LP resonance (right side of the derivative shape).
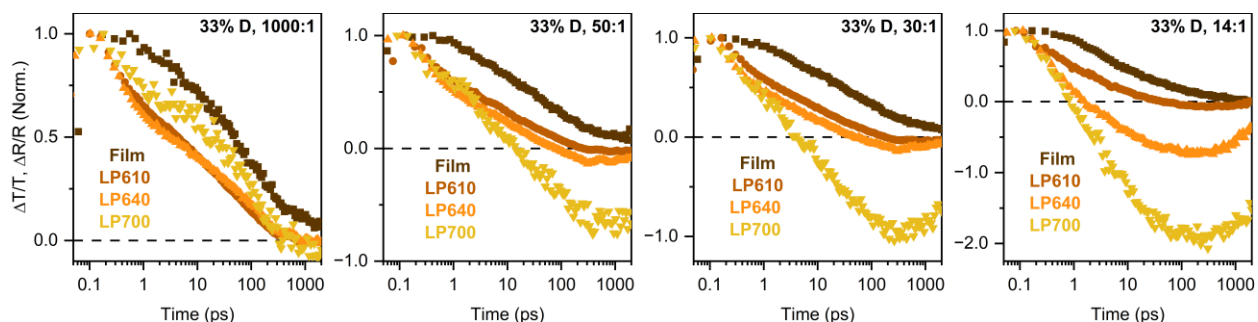
Figure S21: Detuning dependence: extracted kinetics for bare films and microcavities with different **D:A** (left to right: 1000:1, 50:1, 30:1, 14:1). Film kinetics are extracted from the ground state bleach (GSB) peak of **D**, while all microcavity kinetics are selected at the positive features around LP resonance (right side of the derivative shape).
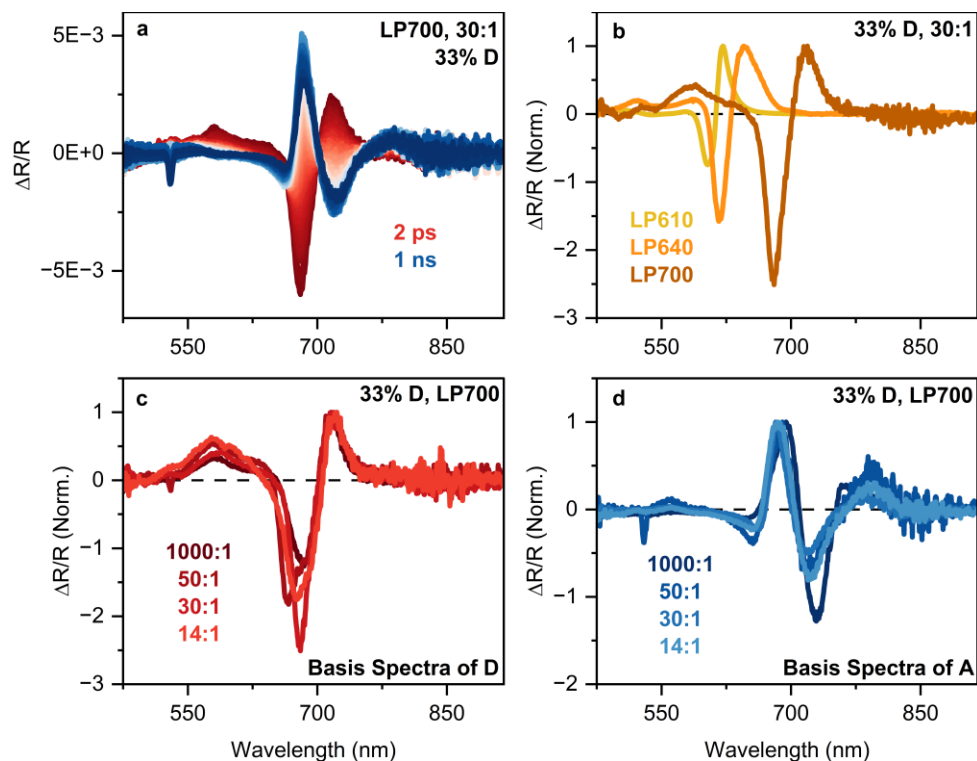
Figure S22: Representative basis spectra of **D** and **A**, used to spectrally decompose TA data. **a)** Raw TA spectra for 33% **D**, 30:1 microcavity with LP700. At earlier times, **D** features (red) are dominant. The flipped shape that reflects the **A** population emerges at later times (blue). **b)** The basis spectra of **D** extracted from individual TA heatmaps with varying detuning, for 33% **D** 30:1. **c)** Basis spectra of **D** and **d) A** extracted for different **D:A** microcavities. The extracted lineshapes are highly reproducible between cavities at a given detuning (here, LP700).
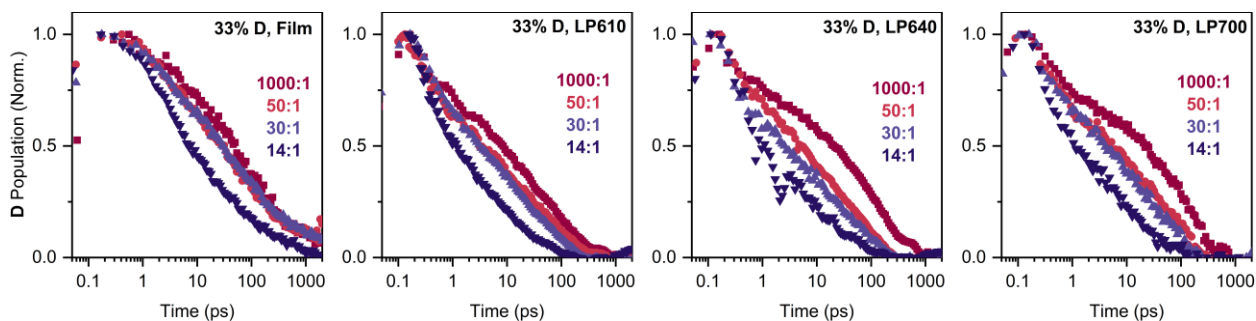

Figure S23: Concentration dependence – **D** population decay in bare films and microcavities with different detunings (left to right: film, 610, 640, 700 nm), *after spectral decomposition*
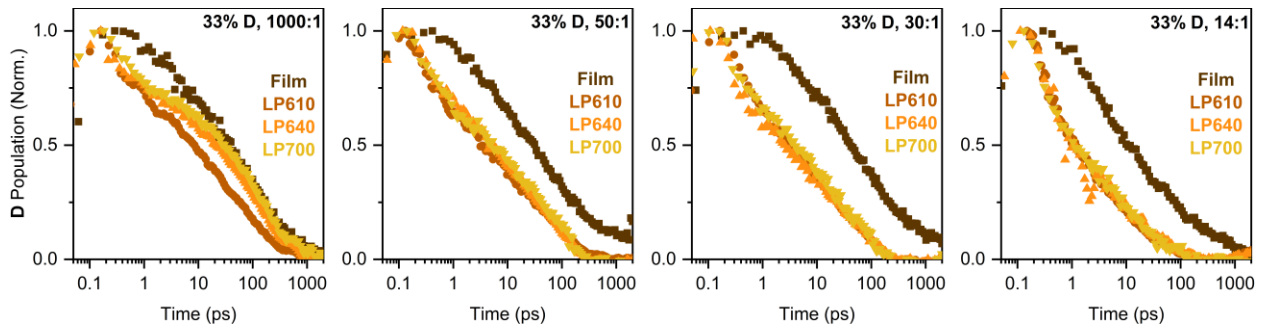
Figure S24: Detuning dependence – **D** population decay in bare films and microcavities with different **D**:**A** (left to right: 1000:1, 50:1, 30:1, 14:1), *after spectral decomposition*. We no longer observe significant detuning dependence after spectrally decomposing the transient absorption spectra.
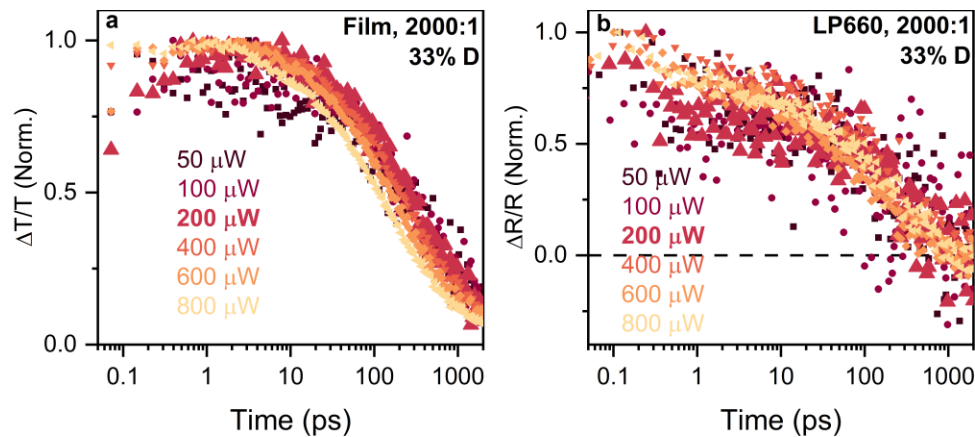
Figure S25: Excitation power dependence measurements for **a)** bare film and **b)** microcavity (**D**:**A** 2000:1). The excitation power used in the TA experiments reported in the main text and analysis above does not exceed *200 ~~μm~~μW*, for bare films or strongly coupled microcavities.

Supplementary Section 5: Rate model

Figure S26: We constructed our rate model based on the four diagrams given above, showing different structures of bare films and microcavities. *a)* Rate model diagram for **D**-only film. S_0 and S_1 levels of **D** are given. k_{exc} describes the excitation of **D** population from S_0 to S_1, while k_D represents the relaxation back to S_0 (radiative and non-radiative). Using the time-resolved measurements performed on 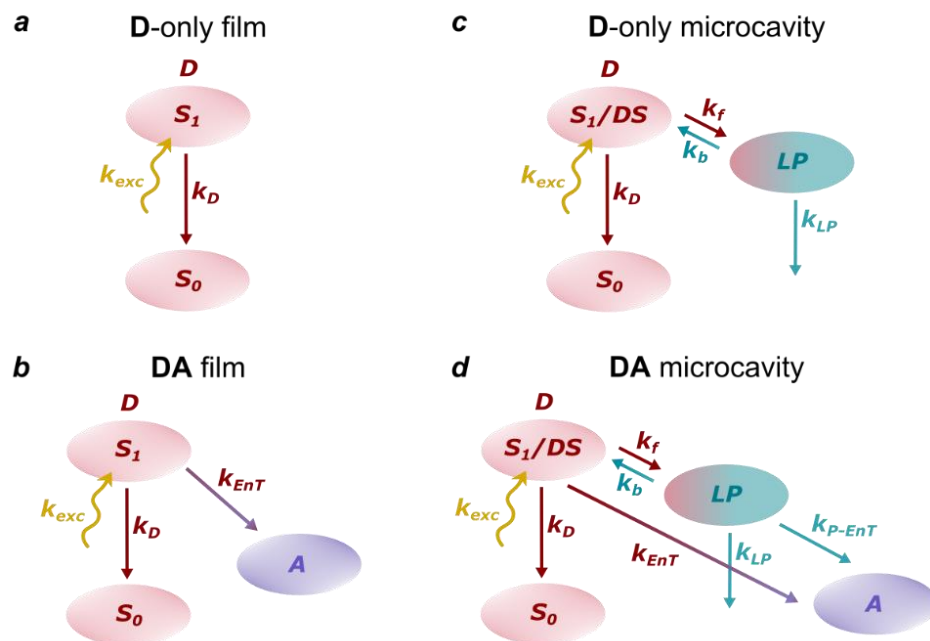**D**-only films, we obtain the rate constant k_D. *b)* Rate model diagram for **DA** film. Moving from **D**-only to **DA** film, we introduce the rate constant k_{EnT}, which describes the energy transfer process from **D** to **A**. Using the TA kinetics of a **DA** film with 14:1 **D:A** and k_D obtained from **a**, we extract the molecular energy transfer rate (k_{EnT}). *c)* Rate model diagram for **D**-only microcavity. Here, in addition to the molecular processes outlined for **D**-only film, we incorporate an equilibrium term between dark states (DS) and lower polariton (LP). The equilibrium is described by the forward and back transfer rates (k_f, k_b). Polariton relaxation is given by k_{LP}, and the polariton lifetime should be <10 fs based on the quality factor of our microcavities. Since the values of k_D and k_{LP} are determined, we can use the rate model for the **D**-only microcavity to gain further insight into the equilibrium. We scan the parameters k_f and k_b to reveal the required conditions that reproduce the necessary behavior. As we observe from TA measurements that **D** population decay in **D**-only films versus microcavities shows no significant difference, we use the **D**-only film decay kinetics as the target output. *d)* We combine all the processes given in the steps above to model the **DA** microcavity. As k_D, k_{EnT}, k_{LP} and k_f:k_b are already established, we turn to polaritonic energy transfer (k_{P-EnT}). We vary k_{P-EnT} to obtain the target output that is based on **D** population decay in 14:1 **D:A** microcavity. Doing so, we pin down the parameters k_f, k_b, and k_{P-EnT}, that can reproduce our experimental observations.
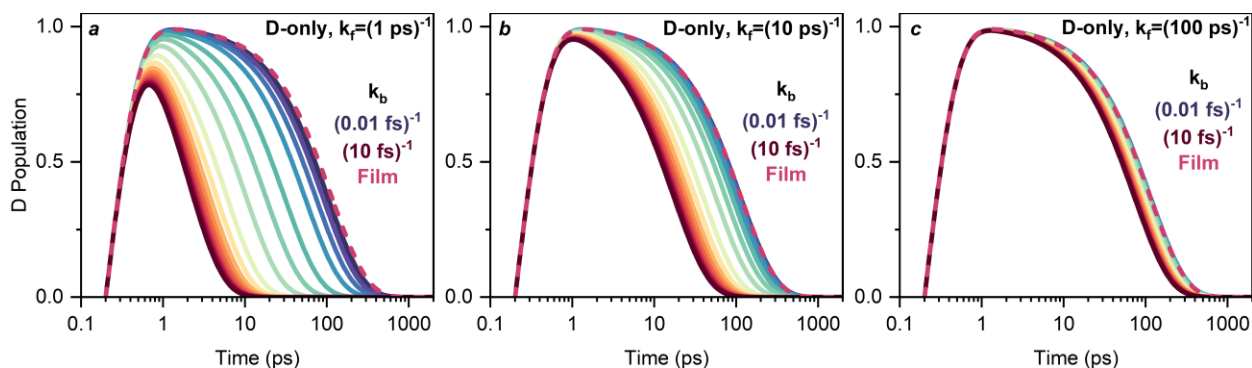
Figure S27: Varying k_b with **a)** k_f = (1 ps)$^{-1}$, **b)** (10 ps)$^{-1}$, and **c)** (100 ps)$^{-1}$ for **D**-only microcavity. The dashed pink line indicates the rate model equivalent of the **D**-only film decay, which is the target output for **D**-only microcavities (since experimentally their dynamics are nearly indistinguishable). At a set k_f value, the back transfer (k_b) needs to be significantly faster to generate this target behavior. The required ratio is ~100000:1 for k_b:k_f, based on all cases sampled.
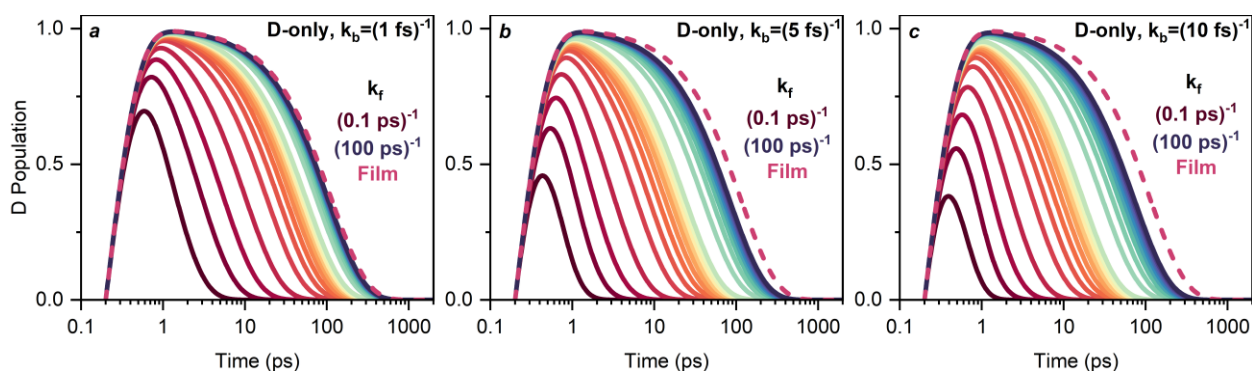

Figure S28: Varying k_f with **a)** k_b = (1 fs)$^{-1}$, **b)** (5 fs)$^{-1}$, and **c)** (10 fs)$^{-1}$ for **D**-only microcavity. The dashed pink line indicates the rate model equivalent of the **D**-only film decay, which is the target output for **D**-only microcavities as above. For back transfer rate of k_b = (1 fs)$^{-1}$, the rate model requires a slow forward transfer rate of (100 ps)$^{-1}$, yielding a ratio of 100000:1 for k_b:k_f. At k_b = (5 fs)$^{-1}$ and (10 fs)$^{-1}$, even the forward rate of (100 ps)$^{-1}$ (equivalent to the bare-molecule decay rate) isn't slow enough to generate the target behavior. This result suggests that either the back-scattering must be markedly faster than photonic leakage from the LP, to prevent too-rapid overall population loss, or the forward scattering is so slow that the **D** population chiefly decays through its intrinsic channels *prior* to scattering. In the latter case, it is not possible to explain the observed effects of strong coupling on energy transfer.
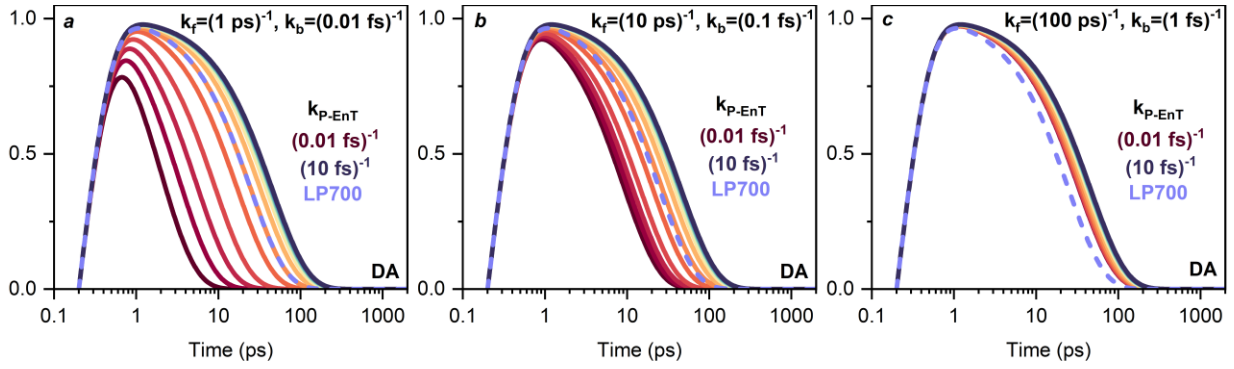
Figure S29: Varying k_{P-EnT} with different pairs of values for k_f and k_b, **a)** $k_f = (1\text{ ps})^{-1}$, **b)** $(10\text{ ps})^{-1}$, and **c)** $(100\text{ ps})^{-1}$. Corresponding k_b values are chosen based on the previously established 100000:1 k_b:k_f ratio. The target output is indicated by dashed purple lines and represents the rate model equivalent of the measured **D** population decay for 14:1 **D:A** microcavity. At $k_f = (100\text{ ps})^{-1}$, it isn't possible to generate the fast decay observed in the experiments for **DA** microcavity. The model requires fast forward transfer rate (k_f) to bring in sufficient population to the LP for polaritons to have an impact on the energy transfer process.
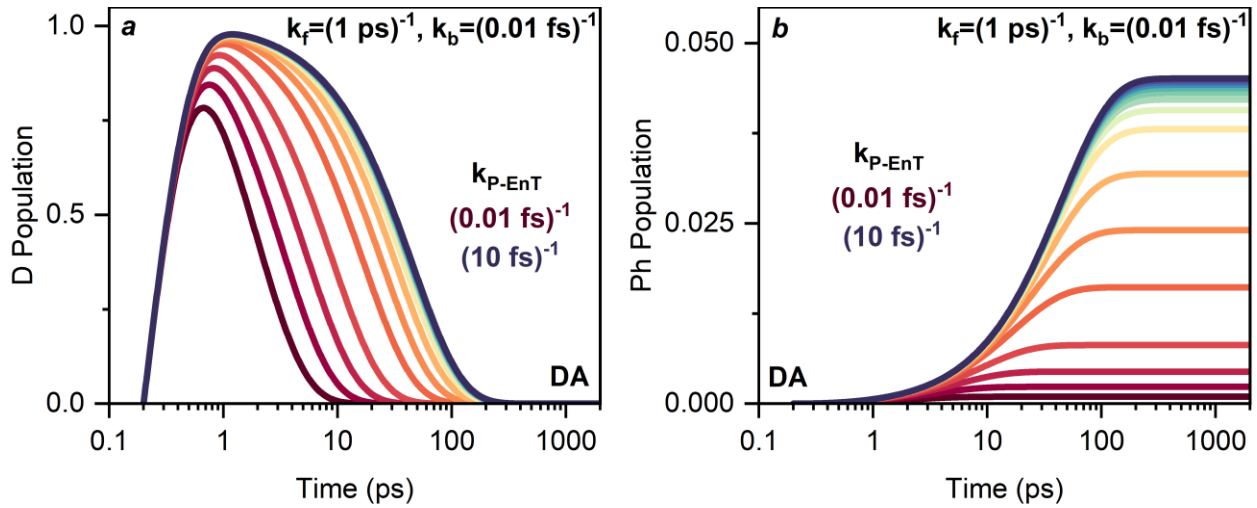
Figure S30: Rate model outputs with varying k_{P-EnT}, displaying the **D** population decay (left) and corresponding **Ph**oton count (right). We observe that for a range of k_{P-EnT} values, the overall population decay of **D** isn't strongly impacted while the change is significant in the photon count. This demonstration supports the experimental observation of no major detuning dependence detected in TA measurements, while such dependence is evident in photoluminescence experiments and Stern-Volmer analysis.
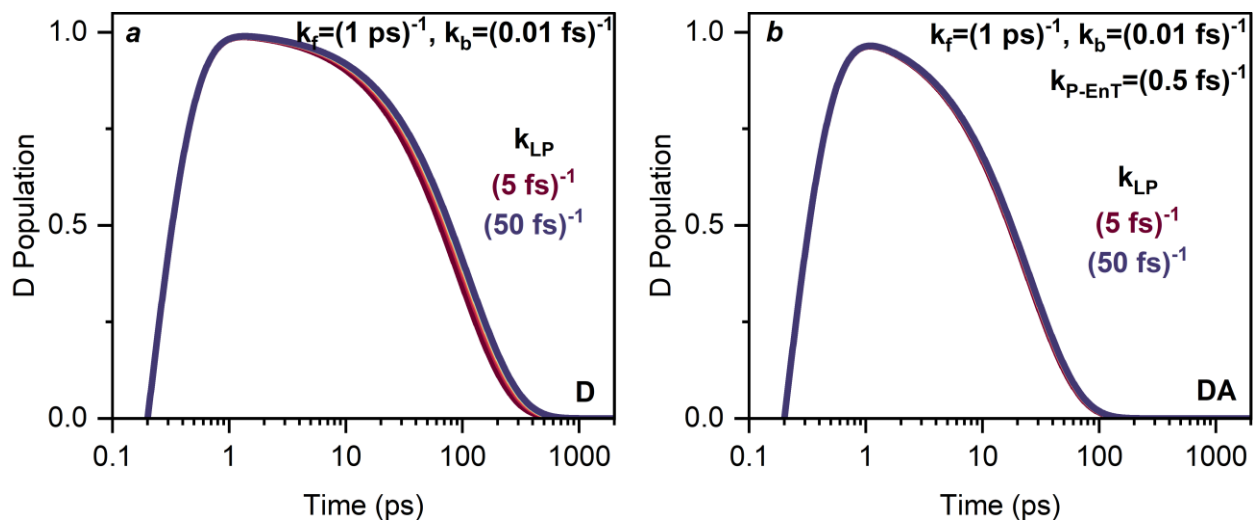
Figure S31: Rate model outputs with varying k_{LP}, displaying the **D** population decay in **D**-only (left) and **DA** microcavity (right). The rate model outputs demonstrate that **D** population decay doesn't display any significant dependence on k_{LP}, and therefore Q-factor, within the range of polariton lifetimes of 5 – 50 fs.

Table S1: Rate Equations for Donor-only Microcavity

State	Rate Equation
S_0	$$\frac{dS_0}{dt} = -k_{exc}S_0$$
S_1	$$\frac{dS_1}{dt} = k_{exc}S_0 - k_D S_1 - k_{f,DS}S_1 + k_{b,DS}LP$$
LP	$$\frac{dLP}{dt} = k_{f,DS}S_1 - k_{b,DS}LP - k_{LP}LP$$
Ph	$$\frac{dPh}{dt} = k_{LP}LP$$

Table S2: Rate Equations for Donor-Acceptor Microcavity

State	Rate Equation
S_0	$$\frac{dS_0}{dt} = -k_{exc}S_0$$
S_1	$$\frac{dS_1}{dt} = k_{exc}S_0 - k_D S_1 - k_{f,DS}S_1 + k_{b,DS}LP - k_{EnT}S_1$$
LP	$$\frac{dLP}{dt} = k_{f,DS}S_1 - k_{b,DS}LP - k_{LP}LP - k_{P-EnT}LP$$
A	$$\frac{dA}{dt} = k_{EnT}S_1 + k_{P-EnT}LP$$
Ph	$$\frac{dPh}{dt} = k_{LP}LP$$

Table S3: Initial Conditions

$S_{0,0}$	$S_{1,0}$	LP_0	A_0	Ph_0
1	0	0	0	0

Table S4: Rate constants used in the rate model

k_{exc}	k_D	k_{EnT}	k_{LP}
$(180\,fs)^{-1}$	$(114.8\,ps)^{-1}$	$(87.3\,ps)^{-1}$	$(10\,fs)^{-1}$
$k_{f,DS}$	$k_{b,DS}$	k_{P-EnT}	
$(1\,ps)^{-1}$	$(10\,as)^{-1}$	$(0.5\,fs)^{-1}$	

References

1. Otsuki, S. & Adacid, K. Effect of Moisture on the Aggregation of Methylene Blue and Rhodamine 6G in Poly(N-vinylpyrrolidone) Film. *Polym J* **27**, 655–658 (1995).

2. Rocha, U. *et al.* Reviewing the effect of aggregates in Rhodamine 6G aqueous solution on fluorescence quantum efficiency. *Spectrochim Acta A Mol Biomol Spectrosc* **317**, 124409 (2024).

3. Chapman, M. & Euler, W. B. Rhodamine 6G Structural Changes in Water/Ethanol Mixed Solvent. *J Fluoresc* **28**, 1431–1437 (2018).

4. Szabó, Á., Szöllősi, J. & Nagy, P. Principles of Resonance Energy Transfer. *Curr Protoc* **2**, e625 (2022).